

# Design of $\pi$ -Conjugated Organic Materials for One-Dimensional Energy Transport in Nanochannels

Juan Carlos Sancho-García,<sup>†</sup> Jean-Luc Brédas,<sup>†,‡</sup> David Beljonne,<sup>†,‡</sup> Jérôme Cornil,<sup>†,‡</sup> Roberto Martínez-Álvarez,<sup>§</sup> Michael Hanack,<sup>§</sup> Lars Poulsen,<sup>||</sup> Johannes Gierschner,<sup>†,||</sup> Hans-Georg Mack,<sup>||</sup> Hans-Joachim Egelhaaf,<sup>||</sup> and Dieter Oelkrug<sup>||</sup>

Laboratory for Chemistry of Novel Materials, Center for Research in Molecular Electronics and Photonics, University of Mons-Hainaut, Place du Parc 20, B-7000 Mons, Belgium, School of Chemistry and Biochemistry, Georgia Institute of Technology, Atlanta, Georgia 30332-0400, Institute of Organic Chemistry, University of Tübingen, Auf der Morgenstelle 18, D-72076 Tübingen, Germany, and Institute of Physical and Theoretical Chemistry, University of Tübingen, Auf der Morgenstelle 8, D-72076 Tübingen, Germany

Received: October 11, 2004; In Final Form: January 19, 2005

Various end-substituted distyrylbenzenes have been synthesized to serve as guest molecules in inclusion compounds to promote efficient energy transport along one-dimensional channels. Their optical and photophysical properties have been characterized at both experimental and theoretical levels. All molecules display a large transition dipole moment between the ground state and lowest excited state and hence a short radiative lifetime (on the order of 1–2 ns). They also exhibit a large spectral overlap between the emission and absorption spectra, which enables efficient energy transport between molecules arranged in a head-to-tail configuration in nanochannels. Hopping rates on the order of  $10^{12}$  s<sup>-1</sup> are calculated at a full quantum-chemical level; this is much larger than the radiative lifetimes and opens the way for energy migration over large distances. Changes in the nature of the terminal substituents are found to modulate the optical properties weakly but to impact significantly the energy transfer rates.

## 1. Introduction

Conjugated polymers such as poly(*p*-phenylenevinylene) (PPV) and its derivatives are widely exploited as active layers in organic-based electrooptic devices, such as light-emitting diodes<sup>1–3</sup> or photodiodes and solar cells.<sup>4–7</sup> This has triggered a large number of theoretical and experimental studies aimed at understanding, and ultimately controlling, their solid-state electronic and optical properties.<sup>8</sup> Biosensors based on PPV derivatives have also been designed recently; their operation relies on the quenching or amplification of the PPV emission properties after a specific recognition event.<sup>9–11</sup> The observed ultrahigh sensitivity has been attributed to the high efficiency of the energy transfer processes taking place between conjugated segments belonging to the same or to neighboring polymer chains. Unfortunately, these sensors most often suffer from a lack of control in both the intramolecular and intermolecular order of the polymer chains, which is sensitive to the detailed chemical structure, the synthetic route, and processing conditions (e.g., the solvent used to spin-coat the films or the temperature). Molecular materials self-assembling into highly organized structures appear attractive in this respect; however, they are often subject to emission quenching upon aggregation<sup>12</sup> whereby the excitations get delocalized over several chains and become nonemissive.

These limitations have motivated the inclusion of well-defined molecular compounds in one-dimensional organic and inorganic channels to study energy transfer processes in the absence of

aggregation effects.<sup>13–20</sup> These architectures also potentially provide for highly directional energy transport, which can be driven by the introduction of an energy gradient (i.e., several compounds with decreasing optical gaps) along the channels.<sup>21</sup> Such host–guest systems can thus act as antennas that funnel excitations from one end of the channel to the other extremity where they can be further exploited;<sup>22</sup> for instance, the excitations could be dissociated into electrical charges to design antenna-sensitized solar cells that would mimic photosynthesis in green plants. Encapsulation of conjugated materials into nanochannels also offers the advantage of increased chemical stability<sup>23,24</sup> and enhanced emission properties when the conjugated backbone gets planarized, thus reducing the detrimental impact of torsional modes.<sup>15,25</sup>

Here, we investigate the potential of a series of end-substituted distyrylbenzenes as energy transporters in one-dimensional channels; their chemical structures are displayed in Figure 1. Note that substitution on the central ring or on the vinylene units<sup>12</sup> is excluded in the present syntheses in order to allow the molecules to fit into the channels. The optical and photophysical properties relevant for energy transfer processes and their modulation upon changes in the nature of the terminal substituents have been characterized experimentally in (solid) solution. We have also performed semiempirical quantum-chemical calculations and compared their results to the experimental data to assess the predictive power of the theoretical approach. In particular, we have simulated the vibronic fine structure in the absorption and emission spectra since this governs the degree of spectral overlap; the latter and with an electronic coupling term are the two key ingredients in the Förster energy transfer rates (vide infra). On the basis of spectral overlap and electronic coupling terms calculated at the quantum-

<sup>†</sup> University of Mons-Hainaut.

<sup>‡</sup> Georgia Institute of Technology, Atlanta.

<sup>§</sup> Institute of Organic Chemistry, University of Tübingen.

<sup>||</sup> Institute of Physical and Theoretical Chemistry, University of Tübingen.

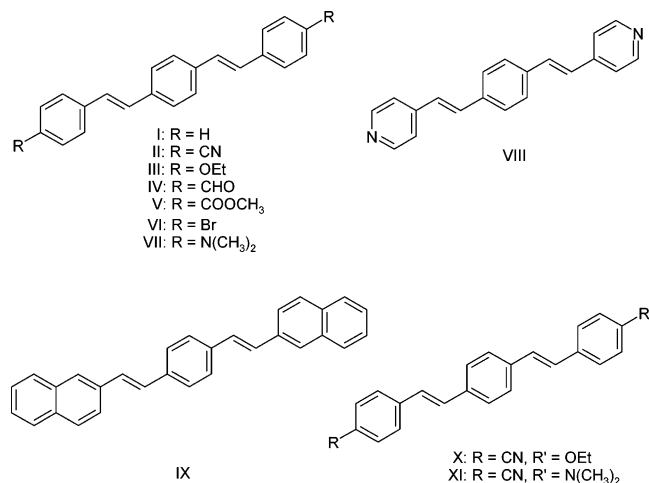


**Figure 1.** Chemical structures of compounds I–XI.

chemical level, we have estimated the nearest-neighbor excitation hopping rates for the various derivatives aligned in a head-to-tail arrangement along the channels.<sup>15,21</sup> Structure–property relationships are established in light of the theoretical results.

## 2. Experimental Section

**2.1. Synthesis of Symmetrically Substituted 4,4'-Distyrylbenzenes.** The target molecules I, II, III, V, VI, VII, and IX have been synthesized via a Wittig reaction of *p*-xylylenebis(triphenylphosphonium bromide) and the appropriate 4-substituted benzaldehyde (for I–VII) or 2-naphthaldehyde (for IX), as described in ref 26 (see Scheme 1 of the Supporting Information). Compound IV has been prepared by a synthetic procedure based on a Wittig reaction between *p*-xylylenebis(triphenylphosphonium bromide) and 4-(diethoxymethyl)benzaldehyde in order to prevent side reactions occurring when terephthaldehyde is used. The obtained solid is then heated in ethanol with diluted aqueous sulfuric acid to liberate the two formyl groups. Compound VIII has been prepared by condensation of 4-methylpyridine with terephthaldehyde in the presence of acetic anhydride and acetic acid<sup>27</sup> (see Scheme 2 of the Supporting Information).

**2.2. Synthesis of Asymmetrically Substituted 4,4'-Distyrylbenzenes.** The first reaction step for the preparation of compound X consists of the Wittig reaction of 4-(diethoxymethyl)benzaldehyde with 4-(ethoxybenzyl)triphenylphosphonium bromide. The obtained solid is boiled in ethanol with diluted sulfuric acid to liberate the protected aldehyde group, thus forming a substituted 4-formylstilbene intermediate which reacts through a second Wittig reaction with 4-(cyanobenzyl)triphenylphosphonium bromide to afford the target compound (see Scheme 2 of the Supporting Information). Compound XI has been prepared from 4-(methylbenzyl)triphenylphosphonium bromide which first reacts with 4-cyanobenzaldehyde to yield the corresponding 4-cyano-4'-methylstilbene. Radicalic bromination with NBS followed by a reaction with triphenylphosphine generates a new phosphonium salt capable of reacting with 4-dimethylaminobenzaldehyde to afford the target molecule (see Scheme 2). After isolation, the compounds are boiled in xylene for several hours in the presence of a trace of iodine to give the pure trans–trans isomer. All the characterization data are available as part of the Supporting Information.

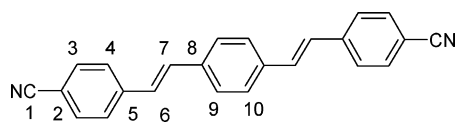
**2.3. Measurements.** UV/vis absorption spectra were measured on a Perkin-Elmer Lambda2 spectrophotometer. Fluorescence emission and excitation spectra were recorded at right angle on a SPEX Fluorolog 222 fluorometer equipped with two

0.25 m double monochromators (1200 lines/mm grating with a spectral resolution of 1.5 nm/mm slit width), a 450 W vertical xenon arc-lamp (Müller Electronics, Germany, model SVX/LAX 1450) and a photomultiplier tube (Hamamatsu, model R928). Fluorescence decays were recorded using a time-correlated single-photon counting setup (pico-timing discriminators (Ortec, model 9307), time-to-amplitude converter (Ortec, model 457), preamplifier (Ortec, model 9306)) utilizing the monochromatic emission of the fluorometer SPEX Fluorolog 222 and the same photomultiplier tube. A picosecond diode laser (PicoQuant, Germany, model LDH-400 (392 nm) or LDH-375 (371 nm), fwhm 70 ps) was used for the excitation. Low-temperature measurements were performed for compound II using a closed cycle Helium cryostat (Kryogenics Technology, model 501A). All experiments were performed in either dioxane, cyclohexane or tetradecane (all Uvasol, Merck) solutions bubbled with nitrogen to remove oxygen. Quantum yields of fluorescence were measured against a 9,10-diphenylanthracene standard (Janssen Chimica, Belgium) in cyclohexane ( $\Phi_F = 0.90$ ).<sup>28</sup>

## 3. Theoretical Methodology

Analysis of vibronic couplings in optical spectra is a topic of ongoing research that has been addressed at various levels of theory. These are challenging calculations because they require an accurate description of the two states involved. Time-dependent density functional theory (TD-DFT) calculations have been recently performed to provide a reliable description of the ground and excited states of various conjugated oligomers.<sup>29,30</sup> However, since calculations on large systems (often encountered in the field of organic electronics) have to balance the required accuracy and the available computational resources, a well-rooted alternative is provided by semiempirical methods. Accordingly, we have exploited them in this study and further assessed their reliability through comparison with Hartree–Fock (HF) and density functional theory (DFT) calculations.

The ground-state geometry ( $S_0$ ) of all compounds has been optimized at the semiempirical Hartree–Fock PM3 (parameterized method 3) level.<sup>31</sup> The PM3 Hamiltonian systematically yields a planar structure while a slight deviation from planarity is calculated at the AM1 (Austin model 1) level; this discrepancy can be attributed to the flatness of the potential energy curve of PPV oligomers with respect to slight torsions along the conjugated backbone.<sup>32,33</sup> The vibrational frequencies have also been computed at the PM3 level, which is recognized as one of the most accurate semiempirical approach for this purpose.<sup>34</sup> The absence of negative frequency values confirms that the planar structure is the global minimum for the various compounds whatever is the starting input geometry; this is fully consistent with the fact that the closely related stilbene molecule is found to be planar both from highly sophisticated theoretical calculations and highly resolved gas-phase fluorescence spectra.<sup>35</sup> The pronounced mirror symmetry observed between the absorption and emission spectra of compound II at low temperature (vide infra) is also a strong indication that the three-ring PPV derivatives studied here are close to planarity, as expected for a terminal substitution of the oligomers. The previous considerations have thus motivated the consideration of fully planar conformers in the ground state knowing that the electronic and optical properties of conjugated materials are slightly affected by small deviations from planarity. We have determined the equilibrium geometry in the lowest excited state ( $S_1$ ) (from which light emission takes place) by coupling the PM3 model to a full CI scheme in a limited active space (PM3-CI), as implemented in the AMPAC package.<sup>36</sup> The size of the

**TABLE 1: Calculated Bond Lengths (Å) and Bond Angles (deg) in the Ground ( $S_0$ ) and Lowest Excited ( $S_1$ ) State of Compound II (See Chemical Structure for Site Labeling), As Obtained at Different Theoretical Levels<sup>a</sup>**

	$S_0$				$S_1$	
	expt	HF/6-311G*	PM3	B3LYP/6-311G*	RCIS/6-311G*	PM3-CI
C <sub>1</sub> –C <sub>2</sub>	1.43	1.441	1.424	1.428	1.436	1.423
C <sub>2</sub> –C <sub>3</sub>	1.41	1.386	1.398	1.402	1.395	1.402
C <sub>3</sub> –C <sub>4</sub>	1.37	1.382	1.388	1.386	1.372	1.381
C <sub>4</sub> –C <sub>5</sub>	1.39	1.393	1.400	1.407	1.410	1.414
C <sub>5</sub> –C <sub>6</sub>	1.44	1.476	1.456	1.461	1.435	1.422
C <sub>6</sub> –C <sub>7</sub>	1.35	1.327	1.343	1.348	1.371	1.382
C <sub>7</sub> –C <sub>8</sub>	1.44	1.474	1.456	1.460	1.416	1.409
C <sub>8</sub> –C <sub>9</sub>	1.39	1.392	1.400	1.406	1.431	1.428
C <sub>9</sub> –C <sub>10</sub>	1.37	1.379	1.387	1.384	1.357	1.367
C <sub>1</sub> –C <sub>2</sub> –C <sub>3</sub>	120	120.1	119.7	120.5	120.2	119.7
C <sub>2</sub> –C <sub>3</sub> –C <sub>4</sub>	120	119.8	119.6	120.0	120.0	119.8
C <sub>3</sub> –C <sub>4</sub> –C <sub>5</sub>	121	121.4	120.4	121.7	121.6	120.5
C <sub>4</sub> –C <sub>5</sub> –C <sub>6</sub>	119	118.4	119.6	118.7	118.8	119.8
C <sub>5</sub> –C <sub>6</sub> –C <sub>7</sub>	126	126.7	123.0	126.9	126.4	122.9
C <sub>6</sub> –C <sub>7</sub> –C <sub>8</sub>	126	127.0	123.1	127.2	126.4	123.2
C <sub>7</sub> –C <sub>8</sub> –C <sub>9</sub>	125	124.0	121.1	124.0	123.9	121.5
C <sub>8</sub> –C <sub>9</sub> –C <sub>10</sub>	122	120.8	120.6	121.0	121.0	121.0

<sup>a</sup> The experimental bond lengths and angles are obtained from X-ray diffraction measurements on single crystals.<sup>78</sup>

CI expansion has been chosen to ensure the convergence of the geometric parameters. The ground-state properties obtained for compound **II** have been compared to DFT<sup>37–39</sup> calculations performed at the hybrid B3LYP level with a 6-311G\* basis set, which combines the Becke exchange<sup>40</sup> and the Lee–Yang–Parr correlation functionals<sup>41</sup> together with an optimized weight for the exact HF exchange.<sup>42</sup>

On the basis of the PM3-optimized structures, the electronic structure of the compounds has been computed by means of the spectroscopic version of the semiempirical Hartree–Fock INDO (intermediate neglect of differential overlap)<sup>43</sup> method, as parametrized with the Mataga–Nishimoto potential for the electron–electron interaction terms. The transition energies and transition dipole moments have been calculated by means of the INDO Hamiltonian coupled to a Single Configuration Interaction (SCI) scheme, in which all the  $\pi$ -occupied and unoccupied levels are involved to generate the configurations. The results obtained for compound **II** have been compared to those provided by ab initio HF calculations (with a 6-311G\* basis set) using GAUSSIAN98<sup>44</sup> in order to judge the reliability of the semiempirical approach; the restricted configuration interaction single (RCIS) level of theory, strictly equivalent to the SCI formalism, has been employed at the HF level for the excited-state characterizations.

#### 4. Reference Calculations

To test the reliability of the cost-effective semiempirical PM3 approach for the oligomers under investigation, the geometric and electronic properties of *p,p'*-dicyanodistyrylbenzene (compound **II**) have also been computed with first-principles techniques. A few selected interatomic distances in the ground [lowest excited] state of this compound are listed in Table 1, as calculated at the HF [HF/RCIS], PM3 [PM3-CI], and B3LYP levels. There is an excellent agreement between the PM3 and B3LYP C–C bond lengths, the maximum deviation being on the order of 0.007 Å. Slightly more pronounced deviations (from 0.004 to 0.020 Å) are observed between the HF and PM3 geometries in both ground and excited states. Table 2 collects

**TABLE 2: Calculated Vibrational Frequencies ( $\nu_k$ , in  $\text{cm}^{-1}$ ) of  $a_g$  Modes in Compound II and Associated Huang–Rhys Factors ( $S_k$ )<sup>a</sup>**

	$\nu_k$			$S_k$	
	B3LYP	HF	PM3	HF	PM3
	127	135	127	0.946	0.464
	444	470	411	0.055	0.004
	756	801	705	0.083	0.009
	1210	1285	1034	0.202	0.021
	1236	1313	1089	0.063	0.001
	1302	1352	1132	0.074	0.002
	1546	1679	1448	0.153	0.018
	1582	1738	1554	0.128	0.000
	1595	1750	1557	0.058	0.015
	1633	1801	1584	0.095	0.375
	1688	1855	1633	0.165	0.631

<sup>a</sup> Only vibrational modes with  $S_k > 0.05$  are listed. The PM3 frequencies are scaled by 0.88 whereas the HF and B3LYP values have not been corrected.

the frequencies of the most active  $a_g$  vibrational modes in the ground state together with the corresponding Huang–Rhys (HR) factors to be used for the simulation of emission spectra; we list here only the modes having an HR factor larger than 0.05. The accuracy of the vibrational frequencies is one of the most severe criteria to assess the reliability of a given theoretical method. The harmonic frequencies calculated at the HF level are known to be systematically overestimated by 10–15%.<sup>45–47</sup> As a result, the use of scaling factors<sup>45</sup> has become popular to overcome the systematic errors linked both to the neglect of anharmonicity effects and to the incomplete description of two-particle effects. Although there is a general consensus for the scaling factor to be used with HF (0.89–0.90) and B3LYP (0.96–0.97) methods, errors in semiempirical calculations are usually less systematic.<sup>48,49</sup> We have thus derived an ad hoc scaling factor for the PM3 method for the set of compounds under study. The value of the scaling factor (equal to 0.88) is based on the comparison between the frequencies extracted from a Franck–Condon analysis of the fluorescence spectrum of a three-ring PPV oligomer (compound **I**), as described in ref 32,

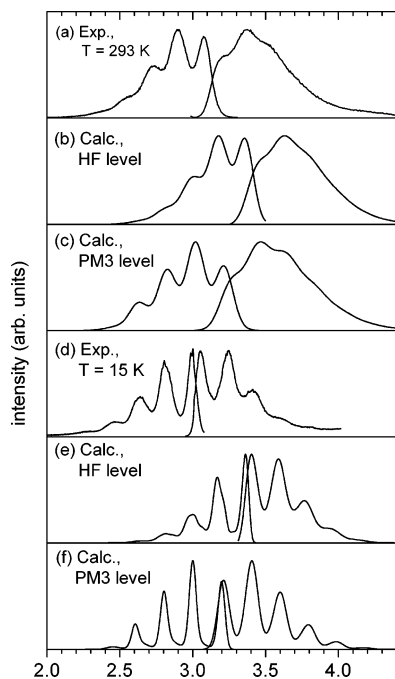


**Figure 2.** Experimental fluorescence emission (left) and excitation (right) spectra of compound **II** in tetradecane at room temperature (a) together with the spectra simulated at the HF (b) and PM3 (c) levels. The theoretical spectra have been broadened by Gaussian functions with a full width at half-maximum (fwhm) chosen to match the experimental resolution ( $1000\text{ cm}^{-1}$  for emission and  $1100\text{ cm}^{-1}$  for absorption). (d–f) Corresponding spectra at 15 K. The fwhm is set here equal to 400 and  $700\text{ cm}^{-1}$  for emission and excitation, respectively. The room temperature excitation spectra are additionally convoluted with an exponential distribution.<sup>32</sup>

and the corresponding PM3 values; the root-mean-square error (RMS) is reduced by a factor of 3 after the scaling procedure. Once this correction is applied to the set of active  $a_g$  modes in the ground state, the difference between the PM3- and B3LYP-calculated values yields a RMS of  $71\text{ cm}^{-1}$  for this oligomer, which is twice as small as the original value. When applied to compound **II**, the scaling leads to a corresponding RMS of  $64\text{ cm}^{-1}$  for the ground-state frequencies. This has triggered the use of the same procedure for the entire set of compounds considered in this study. Analysis of the HR factors shows a substantial change in the contributions of the respective modes between the PM3 and HF results; both approaches point, however, to a dominant contribution arising from a few in-plane  $a_g$  vibrational modes in the regions around  $130\text{ cm}^{-1}$  and  $1600\text{--}1800\text{ cm}^{-1}$ , although the active participation of other C–C stretching and bending low-energy modes cannot be excluded.<sup>50</sup>

We have further assessed the reliability of the PM3 method in describing vibronic couplings by comparing the HF- and PM3-simulated absorption and emission spectra to the experimental excitation and emission spectra for compound **II** both at low and room temperature, see Figure 2. The vibronic progressions have been simulated within the displaced and undistorted harmonic oscillators model, involving the vibrational modes that allow for a recovery of the reorganization energy by up to 98%; the general procedure adopted to simulate the spectra and account for the temperature effects has been described in detail in ref 32. We observe an overall good agreement between theory and experiment since not only the spacing between the vibronic bands but also the fine structure is well reproduced by the calculations. We note, however, that HF better describes the relative intensities of the vibronic features. Compound **II** displays a relatively small Stokes shift

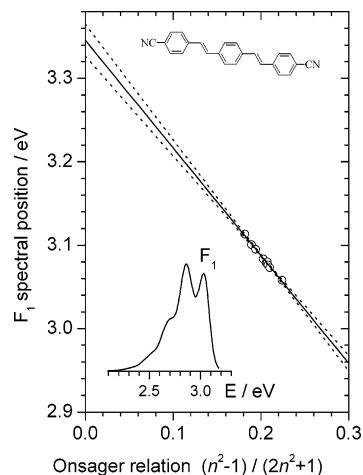


**Figure 3.** Evolution of the spectral position of the 0–0 vibronic band in the fluorescence spectrum of compound **II** in a series of saturated alkanes ( $C_mH_{2m+2}$ ,  $m = 5\text{--}14$ ) as a function of the refractive index  $n$  according to the Onsager relation. Extrapolation to the value in a vacuum was done by linear regression (solid line, 95% confidence intervals are given by the dashed lines).<sup>32</sup>

(defined as the energy difference between the 0–0 peaks in the absorption and emission spectra), which translates into a large spectral overlap between the emission and absorption spectra, as required for efficient energy transfer processes (vide infra).

The additional role of solvent effects is shown in Figure 3, which illustrates the significant evolution of the energy of the 0–0 vibronic feature (referred to as  $F_1$ ) in the fluorescence spectrum of compound **II** as a function of the Onsager factor  $(n^2 - 1)/(2n^2 + 1)$ . Here,  $n$  is the refractive index of different hydrocarbon solvents at the given wavelength. Extrapolation of the spectral position of the  $F_1$  band to  $n = 1$  yields a transition energy of 3.35 eV in a vacuum, which is in excellent agreement with the RCIS/6-311G\* value of 3.38 eV. The large amplitude of the solvent shift ( $\sim 0.3\text{ eV}$ ) clearly advises to consider solvent effects when comparing experimental and ab initio calculated transition energies in electronic spectra. The parametrized INDO/SCI approximation based on the PM3 geometry optimization yields  $\nu_{00} = 3.20\text{ eV}$ , which is slightly larger than the experimental value in common organic solvents ( $\sim 3.1\text{ eV}$ ), see Figure 3.

## 5. Geometric Properties

All derivatives are found to have a fully planar carbon skeleton (with a  $C_{2h}$  symmetry) at the PM3 level in both the  $S_0$  and  $S_1$  states. We note that larger deviations from planarity are expected when substitution occurs on the vinylene moieties<sup>51,52</sup> or the central phenylene ring.<sup>52,53</sup> Here, the terminal substituents exclusively affect the geometry of the rings to which they are connected<sup>54</sup> while the geometry of the vinylene linkages and that of the central ring remain unchanged. The geometry modifications upon excitation into the lowest excited state lead to the appearance of a quinoid character in the rings and to a reduction of the C–C bond alternation in the vinylene units.<sup>55</sup> We have also characterized the extent of  $\pi$ -delocalization in the ground state by referring to the harmonic oscillator model of aromaticity (HOMA) index,<sup>56</sup> defined as:

$$\text{HOMA} = 1 - \frac{\alpha}{m} \sum_i (r_{opt} - r_i)^2, \quad (1)$$

where  $r_i$  is the length of the  $i$ th bond between non-hydrogen



atoms out of the  $m$  involved in the summation. The empirical value for the constant  $\alpha$  (257.7) has been defined in such a way that the HOMA index is equal to 0 for the Kekule structure of a model aromatic system and 1 for the system with all C–C bonds equal to the optimal value  $r_{opt}$  of 1.388 Å. The right-hand side of eq 1 can be cast into the so-called energetic (EN) and geometric (GEO) contributions:<sup>57</sup>

$$\text{HOMA} = 1 - \left[ \alpha(r_{opt} - r_{av})^2 + \frac{\alpha}{m} \sum_i (r_{av} - r_i)^2 \right] = 1 - \text{EN} - \text{GEO} \quad (2)$$

where  $r_{av}$  is the average C–C bond length. This expression reflects that the decrease in the degree of  $\pi$ -delocalization can arise from (i) a deviation of the average bond length with respect to the optimal value (EN) and/or (ii) an increase in the bond-length alternation (GEO). Equation 2 has also been extended to hetero- $\pi$ -electron systems, using the Pauling concept of bond number to average properly the parameters involving the heterogenic atoms.<sup>58</sup> The HOMA index has become one of the most effective ways to quantify the degree of  $\pi$ -delocalization<sup>59,60</sup> over a conjugated fragment. It is calculated here by taking into account all the bonds between heavy atoms, except those involving the terminal substituents. The HOMA index for the unsubstituted three-ring PPV oligomer is calculated to be 0.744 at the PM3 level. A similar calculation based on the B3LYP method, with a cc-pVTZ nearly saturated basis set,<sup>61</sup> provides an index of 0.739, thus confirming the reliability of the PM3 Hamiltonian. All derivatives have a very similar HOMA index, in the 0.735–0.744 range, thus indicating that the terminal substitution only slightly perturbs the  $\pi$ -delocalization along the conjugated backbone.

## 6. Absorption and Emission Properties

The experimental vertical transition energies associated with the emission [lowest absorption] band, which can be readily compared to the theoretical data, have been derived by subtracting [adding] to the electronic origin  $\nu_{00}$  the reorganization energy  $\Delta\nu$  in the ground state [lowest excited]; see Figure 4. The pronounced mirror symmetry observed between the absorption and fluorescence spectra recorded at low temperature indicates that the two components of the reorganization energy are expected to be very similar (see Figure 2). This parameter has been estimated here from the fluorescence spectra at room temperature, in view of its weak thermal evolution, as the difference between the average transition energy and the electronic origin:<sup>32</sup>

$$\Delta\nu = \frac{\int I(\nu)\nu \, d\nu}{\int I(\nu) \, d\nu} - \nu_{00} \quad (3)$$

The corresponding theoretical estimates have been obtained in both the ground and lowest excited states as

$$\Delta\nu(S_0) = E_{S_0/S_1} - E_{S_0} \quad (4)$$

$$\Delta\nu(S_1) = E_{S_1/S_0} - E_{S_1} \quad (5)$$

Here,  $E_{S_0}$  and  $E_{S_1}$  represent the energies of the system in the equilibrium geometry of the ground and lowest excited state, respectively, while  $E_{S_1/S_0}$  [ $E_{S_0/S_1}$ ] is the energy of the lowest excited [ground] state when adopting the ground [lowest excited] state geometry; see Figure 4. The contribution of each vibra-

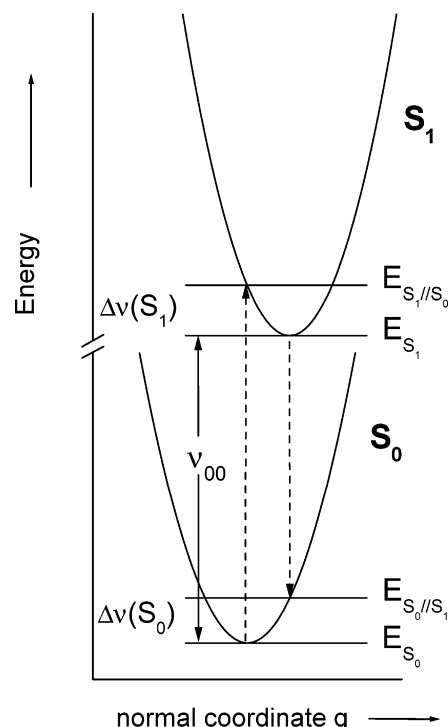


**Figure 4.** Sketch of the potential energy curves in the ground ( $S_0$ ) and lowest excited ( $S_1$ ) states; the reorganization energies  $\Delta\nu$  and the electronic origin  $\nu_{00}$  are also illustrated.

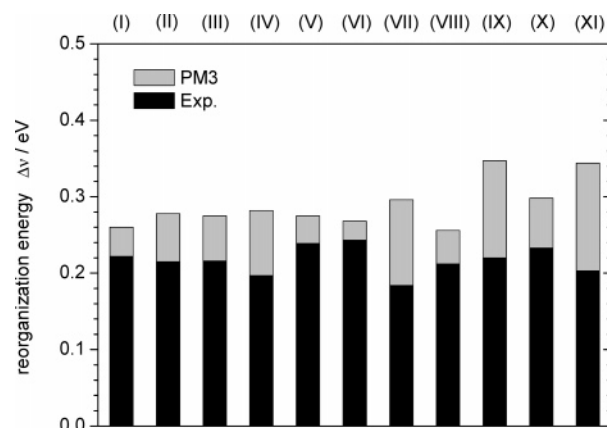


**Figure 5.** Experimental versus PM3-calculated reorganization energies  $\Delta\nu$  for the series of compounds under study.

tional mode to  $\Delta\nu$  can be further determined on the basis of a normal-mode analysis:<sup>62–64</sup>

$$\Delta\nu = \sum_k \nu_k S_k \quad (6)$$

where  $\nu_k$  is the vibrational frequency of the  $k^{\text{th}}$  vibrational mode;  $S_k$  is the Huang–Rhys (HR) factor of the mode, directly related to the change in its normal coordinate between the equilibrium geometries in the  $S_0$  and  $S_1$  states.<sup>65,66</sup> The values obtained from the normal-mode analysis are fully equivalent to those derived from the potential energy surfaces using eqs 4 and 5.<sup>67</sup> We display in Figure 5 the reorganization energies estimated at both theoretical and experimental levels for all derivatives (note that the calculated  $\Delta\nu(S_0)$  and  $\Delta\nu(S_1)$  values are systematically nearly identical, in agreement with the experimental spectra). The two sets of data provide reorganization energies in the range 0.2–0.3 eV for compounds I–VIII; values slightly larger than 0.3 eV are predicted by the calculations for compounds IX–

**TABLE 3: Experimental and INDO/SCI-Calculated Vertical Transition Energies (in eV) for Absorption ( $S_0 \rightarrow S_1$ ) and Emission ( $S_1 \rightarrow S_0$ ) Spectra<sup>a</sup>**

molecule	solvent <sup>b</sup>	expt					calcd		
		$S_0 \rightarrow S_1$	$S_1 \rightarrow S_0$	$\tau_F$	$\Phi_F$	$\tau_0$	$S_0 \rightarrow S_1$	$S_1 \rightarrow S_0$	$\tau_0$
<b>I</b>	D	3.41	2.96	1.39	0.86	1.62	3.59	3.08	0.68
<b>II</b>	D	3.25	2.82	0.99	0.86	1.15	3.48	2.95	0.64
<b>III</b>	D	3.29	2.85	1.10	0.83	1.32	3.52	3.00	0.69
<b>IV</b>	D	3.12	2.72	0.78	0.48	1.62	3.44	2.92	0.65
<b>V</b>	D	3.27	2.79	1.05	0.86	1.22	3.50	2.98	0.65
<b>VI</b>	D	3.38	2.89	0.99	0.72	1.38	3.58	3.06	0.69
<b>VII</b>	C	3.05	2.66	1.03	0.82	1.26	3.47	2.93	0.70
<b>VIII</b>	C	3.45	3.02	0.58	0.40	1.45	3.63	3.12	0.68
<b>IX</b>	D	3.25	2.81	1.16	0.93	1.25	3.48	2.90	0.62
<b>X</b>	C	3.19	2.74	1.18	0.84	1.40	3.48	2.93	0.70
<b>XI</b>	C	2.91	2.49	1.44	0.90	1.60	3.44	2.86	0.74

<sup>a</sup> The natural and fluorescence lifetimes ( $\tau_0$  and  $\tau_F$ , respectively, in ns) as well as the experimental fluorescence quantum yields ( $\Phi_F$ ) are also reported. <sup>b</sup> Solvent used: D = dioxane; C = cyclohexane.

**XI** whereas the experimental estimates lie around 0.2 eV. Note that among all  $a_g$  modes, only a small number couples efficiently to the optically allowed  $S_0-S_1$  ( $1A_g-1B_u$ ) electronic transition within the Franck-Condon approximation.

Table 3 collects the experimental and calculated vertical transition energies for absorption and emission. We observe a good agreement between the two sets of data, except for compounds **VII** and **XI**; in the latter case, the discrepancy observed for absorption (on the order of 0.4 eV) is larger than the typical errors (up to 0.3 eV) made with calculations performed on phenylenevinylene oligomers when neglecting the polarization effects of the surrounding medium. The slightly larger errors found for amino-substituted compounds can be attributed to (i) problems inherent to the nitrogen parametrization in the INDO method and/or (ii) the slight overestimate of the pyramidalization of the nitrogen atom of the dimethylamine group by the PM3 method,<sup>68</sup> which increases the transition by about 0.1 eV compared to a planar geometry. Note also that consideration of torsions along the backbone would further increase the gap between the experimental and theoretical results and can therefore be ruled out as the origin of the discrepancy.

The INDO/SCI-calculated transition energies for compound **VIII** are slightly blue-shifted (by 0.04 eV) with respect to those obtained for the three-ring PPV oligomer **I**. This is rationalized by the fact that the lowest optical transition is mostly described by a HOMO-LUMO excitation in both compounds and that the incorporation of nitrogen atoms leads to a slightly asymmetric stabilization of the HOMO and LUMO levels (by 0.37 and 0.32 eV, respectively, thus increasing the HOMO-LUMO gap). In contrast, the small red shift observed systematically upon substitution for the other compounds primarily results from a decrease in the corresponding HOMO-LUMO gap due to the subtle interplay between the mesomer vs inductive effects of the substituents. These trends are in full agreement with the experimental observations.

The radiative decay rate of the compounds can be estimated at the theoretical level on the basis of absorption and emission integrals following the Strickler and Berg expression:<sup>69</sup>

$$k_f = \frac{8000\pi \ln 10 c_0 n_F^3}{N n_A} \langle \nu_F^{-3} \rangle^{-1} \int_0^\infty \frac{\epsilon(\nu)}{\nu} d\nu \quad (7)$$

where

$$\langle \nu_F^{-3} \rangle^{-1} = \int_0^\infty I_F(\nu) d\nu \left( \int_0^\infty \frac{I_F(\nu)}{\nu^3} d\nu \right)^{-1} \quad (8)$$

Here,  $n_F$  and  $n_A$  are the refractive indices of the solvent at the wavelengths corresponding to the fluorescence and absorption bands, respectively;  $N$  is the Avogadro number,  $c_0$  the velocity of light in a vacuum,  $\epsilon(\nu)$  the molar extinction coefficient, and  $I_F(\nu)$  the intensity of the fluorescence signal at frequency  $\nu$ . Equation 8 can be further manipulated to give an expression that only depends on the vertical fluorescence  $\Delta E_F^{vert} = E_{S_1/S_0} - E_{S_0}$  and absorption transition energies  $\Delta E_A^{vert} = E_{S_0/S_1} - E_{S_1}$  expressed here in  $\text{cm}^{-1}$ :<sup>69</sup>

$$k_f = 0.667 (\Delta E_F^{vert})^3 n^2 \frac{1}{(\Delta E_A^{vert})} f \quad (9)$$

where  $f$  corresponds to the oscillator strength. The natural lifetime (i.e., the inverse of the radiative rate constant) obtained from the INDO/SCI results using this expression (with a value of  $n_{400\text{nm}}^{20\text{K}} = 1.435$  and 1.440 for cyclohexane and dioxane, respectively) are also reported in Table 3. The latter further includes the experimental values of fluorescence quantum yield and of natural and fluorescence lifetimes; note that the radiative decay rate is obtained as the ratio between the fluorescence quantum yield and the fluorescence lifetime.<sup>70</sup> The calculations consistently yield a natural lifetime on the order of 0.6–0.7 ns, in reasonable agreement with the experimental values that range from  $\sim 1.2$  to 1.6 ns. These large values point to the optically allowed nature of the lowest excited state, and hence to the existence of a large transition dipole moment between the ground state and the lowest excited state. We note that the angle made between the transition dipole moment and the long molecular axis of the molecules, defined as the connection line between the terminal carbon atoms of the distyrylbenzene moiety, is estimated to be around  $5^\circ$  at the theoretical level.

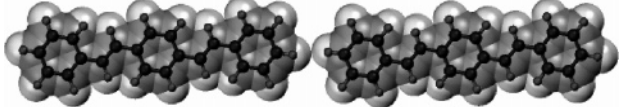
## 7. Energy Hopping Rates

Since all compounds exhibit a strong optical coupling between the ground and the lowest excited state and display hardly any spatial separation between adjacent molecules placed in a head-to-tail arrangement, the Förster mechanism of energy transport is expected to dominate over the orbital overlap-dependent Dexter mechanism. According to Fermi's Golden Rule, the rate  $k_{DA}$  ( $\text{ps}^{-1}$ ) for Förster energy transfer between two chromophores (where one is the excitation donor, D, and the other the excitation acceptor, A) writes:<sup>71</sup>

$$k_{DA} = 1.18 |V_{DA}|^2 J_{DA} \quad (10)$$

where  $V_{DA}$  (in  $\text{cm}^{-1}$ ) represents the electronic coupling between

**TABLE 4:** Calculated Electronic Coupling ( $V_{DA}$ , in  $\text{cm}^{-1}$ ), Spectral Overlap ( $J_{DA}$ , in  $\text{cm}$ ), and Energy Transfer Rate ( $k_{DA}$ , in  $\text{ps}^{-1}$ ) for the Various Compounds under Study, in a Head-to-tail Arrangement and Separated by the van der Waals Distances



molecule	$V_{DA}$	$J_{DA} \times 10^{-5}$	$k_{DA}$
<b>I</b>	234	7.98	5.16
<b>II</b>	191	6.62	2.85
<b>III</b>	107	7.69	1.04
<b>IV</b>	251	6.91	5.14
<b>V</b>	115	7.91	1.23
<b>VI</b>	146	7.59	1.91
<b>VII</b>	147	5.95	1.52
<b>VIII</b>	312	8.65	9.94
<b>IX</b>	178	3.36	1.26
<b>X</b>	128	6.06	1.17
<b>XI</b>	160	3.67	1.11

the initial ( $D^*A$ ) and final ( $DA^*$ ) states, and  $J_{DA}$  (in  $\text{cm}$ ) the overlap between the normalized emission spectrum of the donor and normalized absorption spectrum of the acceptor.  $J_{DA}$  has been calculated here from the absorption and emission spectra simulated at the low-temperature limit, using homogeneous broadenings with a full width at half-maximum of  $550 \text{ cm}^{-1}$ .<sup>32</sup> In view of the strong limitations of the point-dipole model,<sup>72,73</sup>  $V_{DA}$  has been evaluated by means of the distributed monopole method,<sup>74,75</sup> the latter provides an atomic description of the transition dipole moments<sup>73,76</sup> and expresses the electronic coupling as

$$V_{DA} = \frac{1}{4\pi\epsilon_0} \sum_m \sum_n \frac{q_D(m)q_A(n)}{r_{mn}} \quad (11)$$

where  $q_D(m)$  and  $q_A(n)$  represent the atomic transition densities on site  $m$  of the donor and site  $n$  of the acceptor upon excitation to their lowest excited state (considered here to be unrelaxed since there is no excitonic self-localization in short oligomers), as calculated at the INDO/SCI level for the isolated molecules; the summations in eq 11 run over all sites  $m$  of the donor and  $n$  of the acceptor that are separated by a distance  $r_{mn}$ . No attempt has been made to account for the distance-dependent effective screening by the dielectric medium, which is still under discussion.<sup>71</sup> The influence of inhomogeneity, arising from the presence of slightly different molecular conformers with different level energies (*diagonal* disorder) or different molecular orientations within the nanochannels yielding changes in the electronic coupling (*nondiagonal* disorder), will be described elsewhere.

We collect in Table 4 the  $V_{DA}$  and  $J_{DA}$  (in the low-temperature limit) parameters calculated for the various derivatives in a head-to-tail configuration and separated by their van der Waals distance. The energy hopping rates obtained using eq 10 are also reported in Table 4. In all cases, the time scale for transferring an excitation between two adjacent molecules (in the ps range) is much shorter than the radiative lifetime of the compounds (on the order of 1–2 ns), thereby allowing for efficient energy migration over large distances. Analysis of Table 4 indicates that the overlap factor does not vary significantly going from one compound to another; the increase in the transfer rate by up to 1 order of magnitude among the derivatives is actually governed by the evolution of the electronic

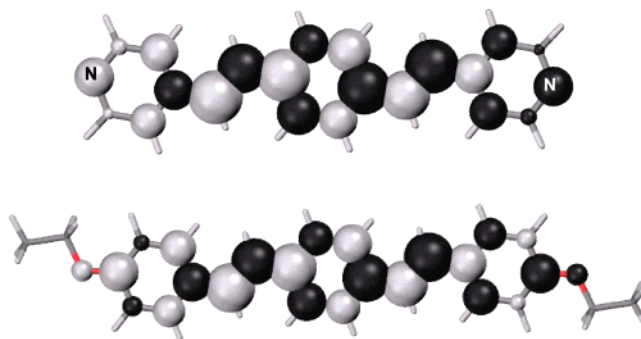


**Figure 6.** INDO/SCI-calculated atomic transition densities associated with the lowest excited state of compounds **VIII** (top) and **III** (bottom). The size and gray scale of the balls reflect the amplitude and sign of the atomic transition densities, respectively.

coupling that varies between 100 and  $300 \text{ cm}^{-1}$ . The highest transfer rate ( $k_{DA} = 9.94 \text{ ps}^{-1}$ ) is obtained for the pyridine-based compound **VIII** and the lowest ( $k_{DA} = 1.04 \text{ ps}^{-1}$ ) for the ethoxy-substituted derivative **III**. At first sight, this might not appear as a huge improvement for a single transfer event; however, this actually leads to a change in the number of possible transfer events during the lifetime of the excitation from about 700 for **III** to 6800 for **VIII**. The evolution of the electronic coupling can be rationalized by examining the distribution of the atomic transition densities plotted in Figure 6 for these two systems. In both cases, the pattern within the conjugated backbone is found to be very similar. However, since there is no contribution arising from the ethyl chains in compound **III**, the average distance between the interacting sites is much larger than in compound **VIII** where the terminal nitrogen atoms have no substituent; this translates into a lower  $V_{DA}$  value for the end-substituted molecule according to eq 11. The energy transfer rates are therefore much more sensitive to the derivatization scheme of the three-ring PPV oligomer rather than to their optical characteristics. A molecular engineering of these compounds can be envisioned to increase further the energy transfer rates.<sup>77</sup>

## 8. Conclusions

In summary, we have synthesized a series of end-substituted distyrylbenzene derivatives and characterized their optical and photophysical properties through a joint experimental and theoretical study. The semiempirical approaches used here have been validated for one of the compounds by a critical comparison to benchmark HF and DFT results, which points to a good compromise between accuracy and computational cost. Relevant parameters for the energy migration have been estimated experimentally and fully support the results of the quantum-chemical calculations. The latter have further been exploited to assess the potentialities of the synthesized compounds as excitation shuttles in one-dimensional nanochannels.

The calculations show that the terminal substituents affect only the geometry of the rings to which they are attached. They also indicate that the substitution leads to a small modulation of the optical properties, typically a small red-shift of the emission and main absorption bands (except for compound **VIII** that incorporates nitrogen atoms), which is consistent with the experimental data. All compounds have a short natural lifetime, on the order of 1–2 ns according to both experimental and theoretical data, and hence a large transition dipole moment between the ground state and the lowest excited state. The absorption and emission spectra simulated with a full account of the vibronic coupling are found to be in good agreement



with the corresponding experimental spectra; they show that the compounds display a moderate Stokes shift, which translates into a large spectral overlap. These optical characteristics allow for efficient energy transport between molecules in a head-to-tail arrangement, as further supported by the fact that the calculated hopping time is much faster than the radiative lifetime ( $\sim 10^{-12}$  vs  $10^{-9}$  s). The energy transfer rates can be further improved by a proper choice of the substitution scheme. In view of the overall good agreement observed between the experimental and theoretical data, our quantum-chemical approach could thus prove to be a cost-effective and reliable tool to design, prior to chemical synthesis, new derivatives with optimized properties.

**Acknowledgment.** The work in Mons has been supported by the Belgian Federal Government "Service des Affaires Scientifiques, Techniques et Culturelles (SSTC)", in the framework of the "Pôle d'Attraction Interuniversitaire en Chimie Supramoléculaire et Catalyse Supramoléculaire (PAI 5/3)", the Belgian National Fund for Scientific Research (FNRS/FRFC) and by the European commission project NANOCHANNEL (Grant No. HPRN-CT-2002-00323). The work at Georgia Tech was partly supported by the National Science Foundation (Grants DMR-0120967 and CHE-0343321) and the IBM Shared University Research Program. The work in Tübingen was supported by the "Fonds der Chemischen Industrie" and by the European commission project NANOCHANNEL. H.-G. Mack thanks the HLRS (Stuttgart, Germany) for access to substantial computer time. R.M.-A. thanks the Alexander von Humboldt Stiftung (Germany) for the reinvention program (2002 and 2003) as well as the "Beca Internacional Universidad Complutense—Flores Valles" (Spain). D.B. and J.C. are FNRS Research Associates. The authors are very grateful to Prof. J. R. Reimers (University of Sydney, Australia) for making available a version of his recently developed DUSHIN program.

**Supporting Information Available:** Schemes 1 and 2 describing the synthetic routes toward compounds I–IX and X–XI, respectively, and text giving the characterization data for all compounds and related references. This material is available free of charge via the Internet at <http://pubs.acs.org>.

## References and Notes

- (1) Burroughes, J. H.; Bradley, D. D. C.; Brown, A. R.; Marks, R. N.; Mackay, K.; Friend, R. H.; Burns, P. L.; Holmes, A. B. *Nature (London)* **1990**, *347*, 539. Friend, R. H.; Gymer, R. W.; Holmes, A. B.; Burroughes, J. H.; Marks, R. N.; Taliani, C.; Bradley, D. D. C.; dos Santos, D. A.; Brédas, J. L.; Lögdlund, M.; Salaneck, W. R. *Nature (London)* **1999**, *397*, 121.
- (2) Gustafsson, H.; Cao, Y.; Treacy, G. M.; Klavetter, F.; Colaneri, N.; Heeger, A. J. *Nature (London)* **1992**, *357*, 477.
- (3) Spreitzer, H.; Becker, H.; Kluge, E.; Kreuder, W.; Schenk, H.; Demandt, R.; Schoo, H. *Adv. Mater.* **1998**, *10*, 1340.
- (4) Sariciftci, N. S.; Smilowitz, L.; Heeger, A. J.; Wudl, F. *Science* **1992**, *258*, 1474.
- (5) Halls, J. J. M.; Walsh, C. A.; Greenham, N. C.; Marseglia, E. A.; Friend, R. H.; Moratti, S. C.; Holmes, A. B. *Nature (London)* **1995**, *376*, 498.
- (6) Brabec, C. J.; Sariciftci, N. S.; Hummel, J. C. *Adv. Funct. Mater.* **2001**, *11*, 15.
- (7) de Boer, B.; Stalmach, U.; Nijland, H.; Hadziioannou, G. *Adv. Mater.* **2000**, *12*, 1581.
- (8) *Primary Photoexcitations in Conjugated Polymers: Molecular Exciton versus Semiconductor Band Model*, Sariciftci, N. S., Ed.; World Scientific Publishing: Singapore, 1997.
- (9) Chen, L.; McBranch, D. W.; Wang, H. L.; Hegelson, R.; Wudl, F.; Whitten, D. G. *Proc. Natl. Acad. Sci. U.S.A.* **1999**, *96*, 12287.
- (10) McQuade, D. T.; Pullen, A. E.; Swager, T. M. *Chem. Rev.* **2000**, *100*, 2537.
- (11) Wang, D.; Gong, X.; Heeger, P. S.; Rininsland, F.; Bazan, G. C.; Heeger, A. J. *Proc. Natl. Acad. Sci. U.S.A.* **2002**, *99*, 49.
- (12) Gierschner, J.; Oelkrug, D. In *Encyclopedia of Nanoscience and Nanotechnology*; Nalwa, H., Ed.; American Scientific Publisher: Stevenson Ranch, CA, 2004; Vol. 8, p 219.
- (13) Hülliger, J.; König, O.; Hoss, R. *Adv. Mater.* **1995**, *7*, 719.
- (14) Bongiovanni, G.; Botta, C.; Brédas, J. L.; Cornil, J.; Ferro, D. R.; Mura, A.; Piaggi, A.; Tubino, R. *Chem. Phys. Lett.* **1997**, *278*, 146.
- (15) Gierschner, J.; Lüer, L.; Oelkrug, D.; Musluoglu, E.; Behnisch, B.; Hanack, M. *Adv. Mater.* **2000**, *12*, 757.
- (16) Gierschner, J.; Lüer, L.; Oelkrug, D.; Musluoglu, E.; Behnisch, B.; Hanack, M. *Synth. Met.* **2001**, *121*, 1695.
- (17) Bongiovanni, G.; Botta, C.; Di Silvestro, G.; Loi, M. A.; Mura, A.; Tubino, R. *Chem. Phys. Lett.* **2001**, *345*, 386.
- (18) Loi, M. A.; Mura, A.; Bongiovanni, G.; Botta, C.; Di Silvestro, G.; Tubino, R. *Synth. Met.* **2001**, *121*, 1299.
- (19) Gierschner, J.; Egelhaaf, H.-J.; Mack, H.-G.; Oelkrug, D.; Martínez Álvarez, R.; Hanack, M. *Synth. Met.* **2003**, *137*, 1449.
- (20) Botta, C.; Destri, S.; Pasini, M.; Picouet, P.; Bongiovanni, G.; Mura, A.; Uslenghi, M.; Di Silvestro, G.; Tubino, R. *Synth. Met.* **2003**, *139*, 791.
- (21) Calzaferri, G.; Huber, S.; Maas, H.; Minkowski, C. *Angew. Chem., Int. Ed.* **2003**, *42*, 3732.
- (22) Huber, S.; Calzaferri, G. *Chem. Phys. Chem.* **2004**, *5*, 239.
- (23) Scaiano, J. C.; García, H. *Acc. Chem. Res.* **1999**, *32*, 783.
- (24) Cardin, D. J. *Adv. Mater.* **2002**, *14*, 553.
- (25) Nijegorodov, N. I.; Downey, W. S. *J. Phys. Chem.* **1994**, *98*, 5639.
- (26) Stammel, C.; Frölich, R.; Wolff, C.; Wenck, H.; de Meijere, A.; Mattay, J. *Eur. J. Org. Chem.* **1942**, *7*, 1709.
- (27) Ichimura, K.; Watanabe, S. *J. Polym. Sci.: Polym. Chem. Ed.* **1982**, *20*, 1419.
- (28) Hamai, S.; Hirayama, F. *J. Phys. Chem.* **1983**, *87*, 83.
- (29) Pogantsch, A.; Heimel, G.; Zojer, E. *J. Chem. Phys.* **2002**, *117*, 5921.
- (30) Dierksen, M.; Grimme, S. *J. Chem. Phys.* **2004**, *120*, 3544.
- (31) Stewart, J. J. P. *J. Comput. Chem.* **1989**, *10*, 209. Stewart, J. J. P. *J. Comput. Chem.* **1989**, *10*, 221. Stewart, J. J. P. *J. Comput. Chem.* **1991**, *12*, 320.
- (32) Gierschner, J.; Mack, H.-G.; Lüer, L.; Oelkrug, D. *J. Chem. Phys.* **2002**, *116*, 8596.
- (33) Claudio, G. C.; Bittner, E. *Chem. Phys.* **2002**, *276*, 81.
- (34) Stewart, J. J. P. In *Encyclopedia of Computational Chemistry*, von Ragué Schleyer, P., Ed.; Wiley: New York, 1998; Vol. 4, p 2579.
- (35) Kwasniewski, S. P.; Claes, L.; François, J.-P.; Deleuze, M. S. *J. Chem. Phys.* **2003**, *118*, 7823.
- (36) Ampac 6.55, Semichem Inc., 7128 Summit, Shawnee, KS 66216, 1997.
- (37) Hohenberg, P.; Kohn, W. *Phys. Rev. B* **1964**, *136*, 864.
- (38) Kohn, W.; Sham, L. J. *Phys. Rev. A* **1965**, *140*, 1133.
- (39) Koch, H.; Holthausen, M. C. *A Chemist's Guide to Density Functional Theory*; Wiley-VCH: Weinheim, Germany, 2000.
- (40) Becke, A. D. *Phys. Rev. A* **1988**, *38*, 3098.
- (41) Lee, C.; Yang, W.; Parr, R. G. *Phys. Rev. B* **1988**, *37*, 785.
- (42) Becke, A. D. *J. Chem. Phys.* **1993**, *98*, 5648.
- (43) Zerner, M. C.; Loew, G. H.; Kichner, R. F.; Mueller-Westerhoff, U. T. *J. Am. Chem. Soc.* **1980**, *102*, 589. Zerner, M. C. In *Reviews in Computational Chemistry*; Lipkowitz, K. W., Boyd, D. B., Eds.; VCH: New York, 1994; Vol. 2, p 313.
- (44) Frisch, M. J.; Trucks, G. W.; Schlegel, H. B.; Scuseria, G. E.; Robb, M. A.; Cheeseman, J. R.; Zakrzewski, V. G.; Montgomery, J. A., Jr.; Stratmann, R. E.; Burant, J. C.; Dapprich, S.; Millam, J. M.; Daniels, A. D.; Kudin, K. N.; Strain, M. C.; Farkas, O.; Tomasi, J.; Barone, V.; Cossi, M.; Cammi, R.; Mennucci, B.; Pomelli, C.; Adamo, C.; Clifford, S.; Ochterski, J.; Petersson, G. A.; Ayala, P. Y.; Cui, Q.; Morokuma, K.; Malick, D. K.; Rabuck, A. D.; Raghavachari, K.; Foresman, J. B.; Cioslowski, J.; Ortiz, J. V.; Stefanov, B. B.; Liu, G.; Liashenko, A.; Piskorz, P.; Komaromi, I.; Gomperts, R.; Martin, R. L.; Fox, D. J.; Keith, T.; Al-Laham, M. A.; Peng, C. Y.; Nanayakkara, A.; Gonzalez, C.; Challacombe, M.; Gill, P. M. W.; Johnson, B. G.; Chen, W.; Wong, M. W.; Andres, J. L.; Head-Gordon, M.; Replogle, E. S.; Pople, J. A. *Gaussian 98*, revision A.10. Gaussian, Inc.: Pittsburgh, PA, 1998.
- (45) Scott, A. P.; Radom, L. *J. Phys. Chem.* **1996**, *100*, 16502.
- (46) Martin, J. M. L.; El-Yazal, J.; François, J. P. *J. Phys. Chem.* **1996**, *100*, 15358.
- (47) Halls, M. D.; Velkovski, J.; Schlegel, H. B. *Theor. Chem. Acc.* **2001**, *105*, 413.
- (48) Thiel, W. *Adv. Chem. Phys.* **1996**, *93*, 703.
- (49) Thiel, W. In *Modern Methods and Algorithms of Quantum Chemistry*; Grotendorst, J., Ed.; John von Neumann Institute for Computing: Jülich, Germany, 2000; p 235.
- (50) Malagoli, M.; Coropceanu, V.; da Silva Filho, D. A.; Brédas, J. L. *J. Chem. Phys.* **2004**, *120*, 7490.
- (51) de Souza, M. M.; Rumbles, G.; Gould, I. R.; Amer, H.; Samuel, I. D. W.; Moratti, S. C.; Holmes, A. B. *Synth. Met.* **2000**, *111–112*, 539.



- (52) Oelkrug, D.; Tompert, A.; Gierschner, J.; Egelhaaf, H.-J.; Hanack, M.; Hohloch, M.; Steinhuber, E. *J. Phys. Chem. B* **1998**, *102*, 1902.
- (53) Hohloch, M.; Maichle-Mössner, C.; Hanack, M. *Chem. Mater.* **1998**, *10*, 1327.
- (54) Cornil, J.; dos Santos, D. A.; Beljonne, D.; Brédas, J. L. *J. Phys. Chem.* **1995**, *99*, 5604.
- (55) Beljonne, D.; Shuai, Z.; Friend, R. H.; Brédas, J. L. *J. Chem. Phys.* **1995**, *102*, 2042.
- (56) Kruszewski, J.; Krygowski, T. M. *Tetrahedron Lett.* **1972**, 3839.
- (57) Krygowski, T. M.; Cyrański, M. *Tetrahedron* **1996**, *52*, 1713.
- (58) Krygowski, T. M.; Cyrański, M. *Tetrahedron* **1996**, *52*, 10255.
- (59) Krygowski, T. M.; Cyrański, M. *Chem. Rev.* **2001**, *101*, 1385.
- (60) Poater, J.; Fradera, X.; Durán, M.; Solá, M. *Chem.—Eur. J.* **2003**, *9*, 1113.
- (61) Dunning, T. H.; Peterson, K. A.; Woon, D. E. In *Encyclopedia of Computational Chemistry*; Schleyer, P. v. R., Ed.; Wiley: New York, 1998; Vol. 1, p 88.
- (62) Negri, F.; Zgierski, Z. *J. Chem. Phys.* **1994**, *100*, 2571.
- (63) Gruhn, N. E.; da Silva Filho, D. A.; Bill, T. G.; Malagoli, M.; Coropceanu, V.; Kahn, A.; Brédas, J. L. *J. Am. Chem. Soc.* **2002**, *124*, 7918.
- (64) Coropceanu, V.; Malagoli, M.; da Silva Filho, D. A.; Gruhn, N. E.; Bill, T. G.; Brédas, J. L. *Phys. Rev. Lett.* **2002**, *89*, 275503.
- (65) Henry, B. R.; Siebrand, W. In *Organic Molecular Photophysics*; Birks, J. B., Ed.; John Wiley & Sons: London, 1973.
- (66) Reimers, J. R. *J. Chem. Phys.* **2001**, *115*, 9103.
- (67) Coropceanu, V.; André, J. M.; Malagoli, M.; Brédas, J. L. *Theor. Chem. Acc.* **2003**, *110*, 59.
- (68) Stewart, J. J. P. In *Encyclopedia of Computational Chemistry*; Schleyer, P. v. R., Ed.; Wiley: New York, 1998; Vol. 3, p 2080.
- (69) Strickler, S. J.; Berg, R. A. *J. Chem. Phys.* **1962**, *37*, 814.
- (70) Lakowicz, J. R. *Principles of Fluorescence Spectroscopy*, 2nd ed.; Kluwer Academic/Plenum Publishers: New York, 1999.
- (71) Scholes, G. D. *Annu. Rev. Phys. Chem.* **2003**, *54*, 57.
- (72) Murell, N.; Tanaka, J. *Mol. Phys.* **1964**, *7*, 634.
- (73) Beljonne, D.; Cornil, J.; Silbey, R.; Millié, P.; Brédas, J. L. *J. Chem. Phys.* **2000**, *112*, 4749.
- (74) Krueger, B. P.; Scholes, G. D.; Fleming, G. R. *J. Phys. Chem. B* **1998**, *102*, 5378.
- (75) Marguet, S.; Markovitsi, D.; Millié, P.; Sigal, H.; Kumar, S. *J. Phys. Chem. B* **1998**, *102*, 4697.
- (76) Beljonne, D.; Pourtois, G.; Silva, C.; Hennebicq, E.; Herz, L. M.; Friend, R. H.; Scholes, G. D.; Setayesh, S.; Müllen, K.; Brédas, J. L. *Proc. Natl. Acad. Sci. U.S.A.* **2002**, *99*, 10982.
- (77) Sancho-García, J. C.; Poulsen, L.; Gierschner, J.; Martínez-Álvarez, R.; Hennebicq, E.; Hanack, M.; Egelhaaf, H.-J.; Oelkrug, D.; Beljonne, D.; Brédas, J. L.; Cornil, J. *Adv. Mater.* **2004**, *16*, 1193.
- (78) Egelhaaf, H.-J.; et al. To be published.